Pressure Swing Adsorption: A Theoretical Study of Diffusion-Induced Separations

This report examines gas separation by a pressure swing adsorption (PSA) process that exploits differences in intraparticle rates of diffusion, rather than differences in adsorption isotherms. Film and intraparticle diffusion resistances are taken into account, but only the latter is examined closely. Each step of a four-step cycle is incorporated, and concentration profiles within the particles and along the column axis are predicted. Several critical PSA operating conditions, including step times, velocities, and pressures are studied in the context of separation of nitrogen from air with zeolite 4A.

Heung-Soo Shin and K. S. Knaebel
Department of Chemical Engineering
Ohio State University
Columbus, OH 43210

Introduction

Pressure swing adsorption (PSA) resembles many more conventional separation processes in that it was successfully commercialized before the fundamental theories of operation were understood. For example, a common application is separation of air to yield nearly pure oxygen by exploiting the difference in the adsorption isotherms of oxygen and nitrogen, e.g., on zeolite 5A. A converse and more recent application is separation of nitrogen from air by exploiting the differences of diffusion rates, e.g., on zeolite 4A. Thus, a local equilibrium theory can be used for the modeling of oxygen production, but diffusion must be considered for the simulation of nitrogen production.

Equilibrium theories have been suggested by many investigators since the first introduction of PSA by Skarstrom (1960). After the theory presented by Turnock and Kadlec (1971), many modified models were introduced (Shendalman and Mitchell, 1972; Chan et al., 1981; Cheng and Hill, 1983; Flores Fernandez and Kenney, 1983; Knaebel and Hill, 1985). The most recent work has accounted for a binary mixture in which both components may adsorb, while earlier versions were constrained to cases involving a nonadsorbing carrier and/or diluent level adsorbate.

A dynamic model including finite mass transfer resistance was first developed by Mitchell and Shendalman (1973). A similar model was suggested by Carter and Wyszynski (1983). Chihara and Suzuki (1983) proposed a similar model, but theirs also considered the energy balance. Raghaven et al. (1985) presented a model that included both pressure-dependent mass transfer coefficients and axial dispersion in an isothermal system. It is important to note that all of these models assumed that the mass transfer rate was represented by a linear driving force (LDF). Hence, intraparticle concentration profiles were not predicted, and the overall mass transfer coefficient in those models included the effect of intraparticle diffusion and depended on the size and type of adsorbent.

In a study closely related to the present work, Raghavan and Ruthven (1985) proposed a general model that also accounted for intraparticle diffusion by the LDF approach. One purpose of their study was to understand kinetically controlled bulk gas separation. Unfortunately, their theory neglected sorption during steps in which pressure varied. Although this may be reasonable for applications involving trace adsorbates in a carrier, this approximation seems unrealistic for bulk gas separations, such as air separation.

The applicability of the LDF model for PSA processes was studied by Nakao and Suzuki (1983). By simulating the cyclic adsorption and desorption within a spherical particle, they have shown that the proportionality parameter in the LDF model, i.e., Ω in $k = \Omega D_e/r_o$, depends on cycle time. The dependence was recently confirmed by Raghavan et al. (1986) through simulation of PSA air-drying with alumina as the adsorbent. For various applications one might expect that Ω would vary with adsorbent and adsorbate properties in a complex manner. Thus, detailed simulation and/or experimental work would be necessary to ascertain its correct value.

Recently, Doong and Yang (1986) incorporated local equilibrium, pore diffusion, and surface diffusion, along with energy balance equations, into successively more sophisticated models. In their nonequilibrium models they assumed parabolic concentration profiles within the adsorbent particles. Although this approach is reasonable in many instances, certain conditions make this approach invalid, as shown later. Do and Rice (1986) also considered the validity of the parabolic profile assumption, but the cases they chose for analysis did not correspond to the application studied here.

Virtually all those prior studies examined cases that were constrained by the rate of diffusion in attainment of a separation in which selectivity was based on equilibrium properties, the paper by Raghavan and Ruthven (1985) being the exception. The present work, however, is concerned with separations that exploit different intraparticle diffusion rates. The purpose is to examine the mechanisms and conditions in order to understand the behavior of each step, and thereby the performance, of the entire PSA cycle. A general model that accounts for intraparticle diffusion and axial dispersion for an isothermal, four-step PSA process is proposed. The mathematical model is solved by orthogonal collocation in which radial profiles in the particles and axial profiles in the bed are considered.

An application of commercial interest that exemplifies the nature of these phenomena is nitrogen production from air with zeolite 4A. In that application oxygen diffuses faster than nitrogen through the zeolite micropores, but it adsorbs less strongly. These conflicting tendencies make the separation both difficult to accomplish in actual practice and difficult to predict. Therefore, the results of the mathematical model are illustrated through a case study of that separation.

Theory

Process description

The process considered here utilizes two identical columns packed with adsorbent. These are connected and operated in a four-step cycle as shown in Figure 1A and 1B. During step 1 feed is supplied at high pressure to bed 1 where adsorption of the faster diffusing component occurs. The other component is removed as a relatively pure product. A portion of this product is throttled to low pressure for purging bed 2. In step 2, bed 1 undergoes blowdown through the feed end, and bed 2 is pressurized with feed. These steps are repeated in steps 3 and 4 except that the points of feed introduction, purge, and blowdown are reversed with respect to beds 1 and 2. A number of minor modifications of this cycle are possible. One that is also considered here is pressurization with product rather than feed. Also, a variety of conditions may be used, giving rise to terminology such as vacuum swing adsorption.

Mathematical model for a single column

The model is based on the following assumptions:

1. The bed is isothermal.
2. The pressure drop through the adsorbent bed is negligible.
3. The adsorption equilibrium isotherm is linear.
4. The flow pattern is described by the axially dispersed, plug flow model.
5. The adsorbent particle is considered to be a uniform sphere.

Under these assumptions, the material balances for the components of a binary mixture, A (e.g., O_2) and B (e.g., N_2), within an adsorbent particle are given by ($i = A$ or B):

$$\frac{\partial q_i}{\partial t} = D_{ei}\left(\frac{\partial^2 q_i}{\partial r^2} + \frac{2}{r}\frac{\partial q_i}{\partial r}\right) \tag{1}$$

The particle boundary conditions are:

$$\left.\frac{\partial q_i}{\partial r}\right|_{r=0} = 0 \tag{2}$$

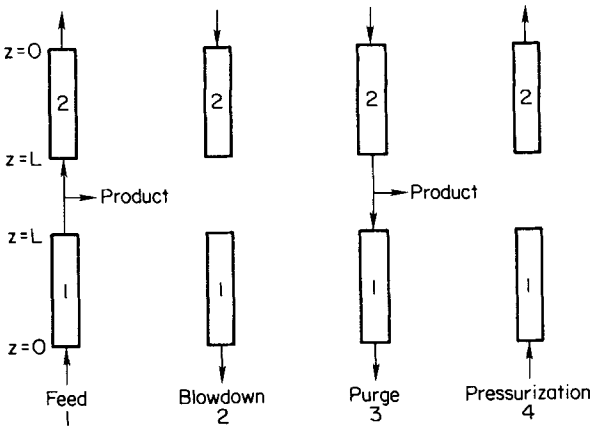

Figure 1A. Basic four-step PSA cycle.
Step names and numbers are shown for column 1; column 2 is 180° out of phase

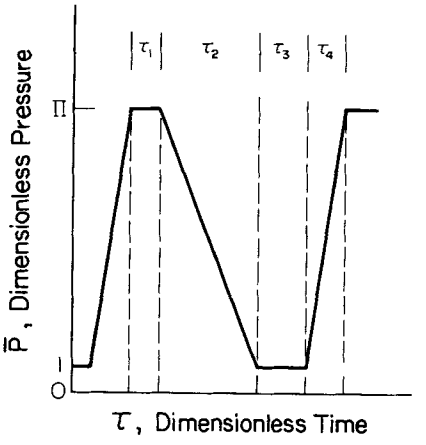

Figure 1B. Pressure swing pattern.

$$D_{ei}\left.\frac{\partial q_i}{\partial r}\right|_{r=r_o} = k_i\left(C_i - \frac{q_i|_{r=r_o}}{K_i}\right) \tag{3}$$

Boundary conditions of Eq. 2 arise from symmetry, and boundary conditions of Eq. 3 describe the film mass transfer between bulk gas phase and adsorbent surface.

The corresponding material balance in the interstitial fluid of the fixed bed is:

$$\frac{\partial C_A}{\partial t} - D_L\frac{\partial^2 C_A}{\partial z^2} + \frac{\partial}{\partial z}(vC_A) = -\frac{1-\epsilon_b}{\epsilon_b}\left[\frac{3k_A}{r_o}\left(C_A - \frac{q_A|_{r=r_o}}{K_A}\right)\right] \tag{4}$$

Note that feed is supplied at $z = 0$ and product is removed at $z = L$. The conventions for flow direction and position are shown in Figure 1A for all of the steps. The well-known Danckwerts boundary conditions are applied for all steps except blowdown, during which no influent is present. For the high-pressure feed step and pressurization step:

$$D_L\left.\frac{\partial C_A}{\partial z}\right|_{z=0} = v(C_A|_{z=0^+} - C_A|_{z=0^-}) \tag{5}$$

$$\left.\frac{\partial C_A}{\partial z}\right|_{z=L} = 0 \tag{6}$$

For the purge step:

$$\left.\frac{\partial C_A}{\partial z}\right|_{z=0} = 0 \tag{7}$$

$$D_L \left.\frac{\partial C_A}{\partial z}\right|_{z=L} = v(C_A|_{z=L^-} - C_A|_{z=L^+}) \tag{8}$$

Note that the fluid velocity is inherently negative during the purge step. For the blowdown step:

$$\left.\frac{\partial C_A}{\partial z}\right|_{z=0} = 0 \tag{9}$$

$$\left.\frac{\partial C_A}{\partial z}\right|_{z=L} = 0 \tag{10}$$

The overall mass balance is obtained as follows:

$$\frac{\partial C}{\partial t} + \frac{\partial}{\partial z}(vC) = -\frac{1-\epsilon_b}{\epsilon_b} \cdot \left[\frac{3k_A}{r_o}\left(C_A - \frac{q_A|_{r=r_o}}{K_A}\right) + \frac{3k_B}{r_o}\left(C_B - \frac{q_B|_{r=r_o}}{K_B}\right)\right] \tag{11}$$

Applying ideal gas law, $C = P/RT$ and $C_B = P/RT - C_A$, Eq. 11 becomes:

$$\frac{\partial v}{\partial z} + \frac{1}{P}\frac{dP}{dt} = -\frac{1-\epsilon_b}{\epsilon_b} \cdot \frac{RT}{P} \cdot \left[\left(\frac{3k_A}{r_o} - \frac{3k_B}{r_o}\right)C_A - \frac{3k_A}{r_o}\frac{q_A|_{r=r_o}}{K_A} + \frac{3k_B}{r_o}\left(P/RT - \frac{q_B|_{r=r_o}}{K_B}\right)\right] \tag{12}$$

Stipulated boundary conditions that arise from the operating policy are:

$$\text{High-pressure feed step} \quad v|_{z=0} = v_H \tag{13}$$

$$\text{Blowdown step} \quad v|_{z=L} = 0 \tag{14}$$

$$\text{Purge step} \quad v|_{z=L} = v_L \tag{15}$$

$$\text{Pressurization step} \quad v|_{z=L} = 0 \tag{16}$$

Insertion of $\partial v/\partial z$ from Eq. 12 into Eq. 4 gives:

$$\frac{\partial C_A}{\partial t} - D_L\frac{\partial^2 C_A}{\partial z^2} + v\frac{\partial C_A}{\partial z} - \frac{1-\epsilon_b}{\epsilon_b}\frac{RT}{P}\left(\frac{3k_A}{r_o} - \frac{3k_B}{r_o}\right)C_A^2 + \left[-\frac{1}{P}\frac{dP}{dt} + \frac{1-\epsilon_b}{\epsilon_b}\left(\frac{3k_A}{r_o} - \frac{3k_B}{r_o}\right) + \frac{1-\epsilon_b}{\epsilon_b}\frac{RT}{P}\left(\frac{3k_A}{r_o}\frac{q_A|_{r=r_o}}{K_A} + \frac{3k_B}{r_o}\frac{q_B|_{r=r_o}}{K_B}\right)\right]C_A - \frac{1-\epsilon_b}{\epsilon_b}\frac{3k_A}{r_o}\frac{q_A|_{r=r_o}}{K_A} = 0 \tag{17}$$

Equations 1–3, 5–10, and 12–17 were reduced to dimensionless forms by introducing the following dimensionless variables:

$$Q_A = \frac{q_A}{K_A C_H}, \quad Q_B = \frac{q_B}{K_B C_H}, \quad \bar{C}_A = \frac{C_A}{C_H}, \quad \bar{C}_B = \frac{C_B}{C_H}$$

$$\eta = \frac{r}{r_o}, \quad \chi = \frac{z}{L}, \quad \tau = \frac{D_{eA}t}{r_o^2}, \quad \tau_H = \frac{D_{eA}L}{r_o^2 v_H}$$

$$\lambda_A = \frac{k_A r_o}{D_{eA}K_A}, \quad \lambda_B = \frac{k_B r_o}{D_{eB}K_B}$$

$$\psi_A = K_A\frac{1-\epsilon_b}{\epsilon_b}, \quad \psi_B = K_B\frac{1-\epsilon_b}{\epsilon_b}$$

$$\theta_A = \frac{v_H r_o^2 \epsilon_b}{LD_{eA}K_A(1-\epsilon_b)}, \quad \gamma_D = \frac{D_{eB}}{D_{eA}}, \quad \bar{v} = \frac{v}{v_H}$$

$$\bar{P} = \frac{P}{P_L}, \quad \Pi = \frac{P_H}{P_L}, \quad Pe = \frac{Lv_H}{D_L}, \quad \gamma_v = \frac{v_L}{v_H}$$

The resulting dimensionless particle material balance equations are:

$$\frac{\partial Q_i}{\partial \tau} = \frac{\partial^2 Q_i}{\partial \eta^2} + \frac{2}{\eta}\frac{\partial Q_i}{\partial \eta} \tag{18}$$

with boundary conditions:

$$\left.\frac{\partial Q_i}{\partial \eta}\right|_{\eta=0} = 0 \tag{19}$$

$$\left.\frac{\partial Q_i}{\partial \eta}\right|_{\eta=1} = \lambda_i(\bar{C}_i - Q_i|_{\eta=1}) \tag{20}$$

And the interstitial fluid material balance becomes:

$$\frac{\partial \bar{C}_A}{\partial \tau} - \frac{\psi_A\theta_A}{Pe}\frac{\partial^2 \bar{C}_A}{\partial \chi^2} + \psi_A\theta_A\bar{v}\frac{\partial \bar{C}_A}{\partial \chi} - \frac{3}{\bar{P}}\Pi(\psi_A\lambda_A - \psi_B\lambda_B\gamma_D) \cdot \bar{C}_A^2 + \left[-\frac{1}{\bar{P}}\frac{d\bar{P}}{d\tau} + 3\psi_A\lambda_A - 3\psi_B\lambda_B\gamma_D + \frac{3}{\bar{P}} \cdot (\psi_A\lambda_A\Pi Q_A|_{\eta=1} + \psi_B\lambda_B\Pi\gamma_D Q_B|_{\eta=1})\right]\bar{C}_A - 3\psi_A\lambda_A Q_A|_{\eta=1} = 0 \tag{21}$$

The Danckwerts boundary conditions for the high-pressure feed step and the pressurization step become:

$$\left.\frac{\partial \bar{C}_A}{\partial \chi}\right|_{\chi=0} = Pe\bar{v}(\bar{C}_A|_{\chi=0^+} - \bar{C}_A|_{\chi=0^-}) \tag{22}$$

$$\left.\frac{\partial \bar{C}_A}{\partial \chi}\right|_{\chi=1} = 0 \tag{23}$$

for the purge step:

$$\left.\frac{\partial \bar{C}_A}{\partial \chi}\right|_{\chi=0} = 0 \tag{24}$$

$$\left.\frac{\partial \bar{C}_A}{\partial \chi}\right|_{\chi=1} = Pe\bar{v}(\bar{C}_A|_{\chi=1^-} - \bar{C}_A|_{\chi=1^+}) \tag{25}$$

and for the blowdown step:

$$\left.\frac{\partial \bar{C}_A}{\partial \chi}\right|_{\chi=0} = 0 \tag{26}$$

$$\left.\frac{\partial \bar{C}_A}{\partial \chi}\right|_{\chi=1} = 0 \tag{27}$$

The overall material balance for the interstitial fluid is:

$$\frac{1}{\tau_H}\frac{\partial \bar{v}}{\partial \chi} + \frac{1}{\bar{P}}\frac{d\bar{P}}{d\tau} = -\frac{3\Pi}{\bar{P}}(\psi_A\lambda_A - \psi_B\lambda_B\gamma_D)\bar{C}_A + \frac{3}{\bar{P}}\psi_A\lambda_A\Pi Q_A|_{\eta=1} + \frac{3}{\bar{P}}\psi_B\lambda_B\Pi\gamma_D Q_B|_{\eta=1} - 3\psi_B\lambda_B\gamma_D \tag{28}$$

Finally, the velocity boundary conditions are:

$$\text{High-pressure feed step} \quad \bar{v}|_{\chi=0} = 1 \tag{29}$$

$$\text{Blowdown step} \quad \bar{v}|_{\chi=1} = 0 \tag{30}$$

$$\text{Purge step} \quad \bar{v}|_{\chi=1} = \gamma_v \tag{31}$$

$$\text{Pressurization step} \quad \bar{v}|_{\chi=1} = 0 \tag{32}$$

Solution technique

In order to solve the coupled partial differential equations, an orthogonal collocation method (Villadsen and Michelsen, 1978) was applied for Eqs. 18 to 32. The resulting linear equation and ordinary differential equations were solved by Krout's LU decomposition (Ketter and Prawel, 1969) and Gear's method.

Eight collocation points along the radius of an adsorbent particle and six collocation points along the axis of the bed were necessary to obtain a reasonably accurate solution under the conditions of this study. More collocation points were tested for particular conditions, with as many as ten radial points and eight axial points. Selection of the lower values was based on imperceptible differences in the results, and on the significant advantage of convergence time for fewer points. Using a VAX-11/780 minicomputer, the calculations required two to four CPU hours to reach steady state, depending on the values of parameters. Details of the method are given elsewhere (Shin, 1986).

Case Study

The application studied here was separation of nitrogen from air with zeolite 4A. The characteristics of the adsorbent and packed bed are given in Table 1. For simplicity, the film mass transfer resistance was assumed to be negligible compared to intraparticle mass transfer resistance on zeolite 4A, so a large film mass transfer coefficient was used.

The assumptions cited above are partially justified by work of Matz and Knaebel (1986), who found experimentally that temperature fluctuations for oxygen removal from air by PSA with zeolite 5A are too small to significantly affect the properties. The equilibrium-based selectivity for nitrogen over oxygen is roughly the same in zeolites 4A and 5A, so the temperature shifts should be comparable. Pressure drop calculations by the Ergun equation have indicated that, under the conditions of the subsequent cases, pressure drop is less than 2% of the absolute pressure except in the last case, in which pressurization with product is considered and the pressure drop is then less than 10% of the total absolute pressure. Miller et al. (1986) and Ball (1985) have found that the isotherms of oxygen and nitrogen are nearly linear and, in the former study, independent above 24°C. Data adapted from Ball are shown in Figure 2. Finally, zeolite 4A is commonly produced in spherical form.

Table 1. Characteristics of Adsorbent and Packed Bed

Particle radius	$r_o = 0.094$ cm*
Bed void fraction	$\epsilon_b = 0.40$
Bed length	$L = 121.9$ cm
Eff. diffusivity of O_2	$D_{eA} = 1 \times 10^{-4}$cm^2/s
Eff. diffusivity of N_2	$D_{eB} = 1.6 \times 10^{-6}$cm^2/s
Eff. diffusivity ratio	$\gamma_D = 0.016$**
Isotherm slope of O_2	$K_A = 2.032\left(\frac{\text{mol/cm}^3\text{ solid}}{\text{mol/cm}^3\text{ gas}}\right)$*
Isotherm slope of N_2	$K_B = 5.663\left(\frac{\text{mol/cm}^3\text{ solid}}{\text{mol/cm}^3\text{ gas}}\right)$*
Mass transfer coeff. of O_2	$k_A = 1{,}000$ cm/s
Mass transfer coeff. of N_2	$k_B = 1{,}000$ cm/s
Pressure at purge step	$P_L = 1$ bar

*Data of Ball (1985)
**Based on value estimated from Ruthven and Derrah (1975)

The ratio of effective diffusivities (N_2 to O_2) was taken to be of the order 1:60. The numerical value calculated by the method of Ruthven and Derrah (1975) was even larger than that at 45°C. Subsequently, the effective diffusivity of O_2 (A) was set arbitrarily because, depending on pretreatment and other conditions, experimental values may span three decades. Fortunately, the most important parameter for the separation is the effective diffusivity ratio, not the absolute effective diffusivities. Nevertheless, the absolute effective diffusivity is related to the

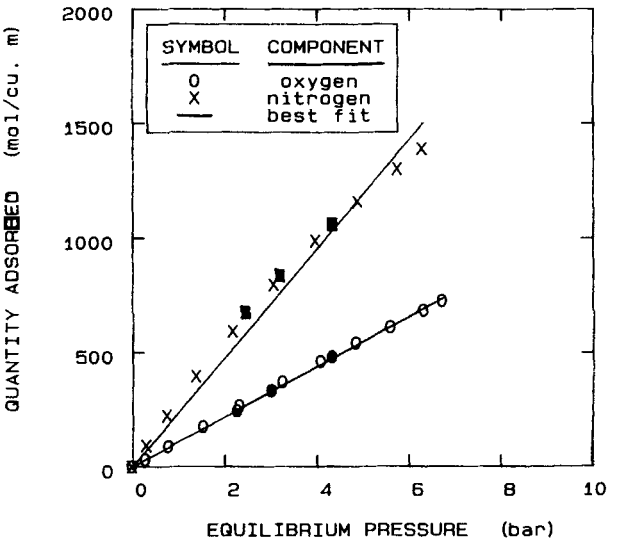

Figure 2. Equilibrium isotherms for N_2 and O_2 on zeolite 4A at 45°C.
O× data obtained by uptake of adsorbate
●■ denote release
Best fit is $q = KC = Kp/RT$.

actual duration of each step of the PSA cycle. Despite that, since dimensionless time was used in the calculation, the overall performance of separation is not affected by the absolute effective diffusivity. A frequent conclusion of diffusion rate studies is that the limiting step is for diffusion in micropores, possibly in the Knudsen regime. In that case, pressure does not affect diffusivity, and that provided justification for omitting that effect.

The pressure swing pattern used in this study is shown in Figure 1B, in which individual steps are identified along with their elapsed times. During the pressurization and blowdown steps, linear pressure changes are assumed, and pressure remains constant during the high-pressure feed and purge steps.

The object of this case study was to gain an understanding of the effects of specific operating conditions and parameters, especially on the quality and quantity of the product. For example, each step interval and other conditions were varied to examine their effects on the separation. Conversely, other pragmatic parameters of performance, e.g., product recovery and adsorbent productivity, were not studied systematically.

General results

Some results of the analysis are shown in Figures 3–6 for nitrogen separation with zeolite 4A using pressurization with feed, and using beds that are initially air-filled. Figure 3 shows the progress of nitrogen mole fraction in the gas phase toward the cyclic steady state. Figure 4 illustrates the gas phase N_2 mole fraction at the end of each step during cyclic steady state. The results show that the region of high-purity product is restricted to the end of the bed during pressurization for $P_L = 1$ bar. The small region of high purity limits the velocity during the high-pressure feed step to a low value in order to get a relatively pure product.

Figures 5 and 6 show the dimensionless intraparticle concentration of oxygen and nitrogen at the end of each step during the cyclic steady state. Due to its relatively high diffusivity, the intraparticle concentration of oxygen changes widely over the entire adsorbent particle. Conversely, the concentration change

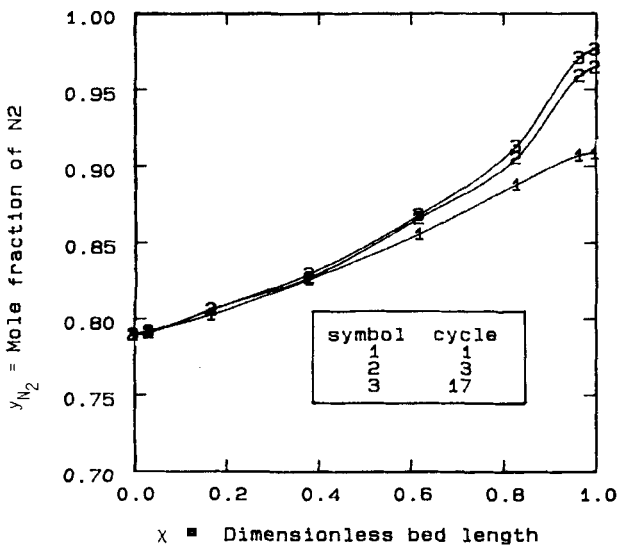

Figure 3. Gas phase N_2 mole fraction in bed at end of high-pressure feed step.
Curves show status at end of indicated cycle

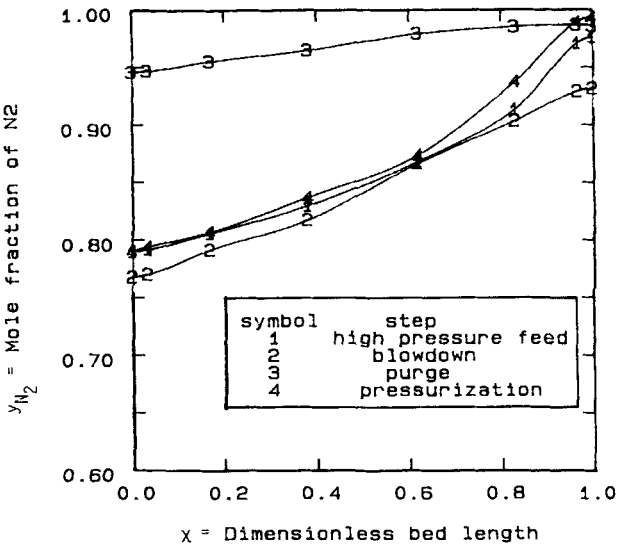

Figure 4. Gas phase mole fraction of N_2 in bed at cyclic steady state at the end of indicated step.

of nitrogen is restricted to dimensionless radii greater than 0.7. The concentration in the interior (radii less than 0.7) remains nearly constant. As a result, if the above assumptions and conditions are valid, presumption of a parabolic concentration profile within a particle will give poor results for diffusion-induced PSA separations. This finding is an exception to the approach of Doong and Yang (1986), and to the cases chosen for study by Do and Rice (1986).

Specific comparisons

Effect of Inlet Velocity and Duration of High-Pressure Feed Step. The parameters v_H and τ_1 are directly related to the purity of product because the pure gas produced during the pressuriza-

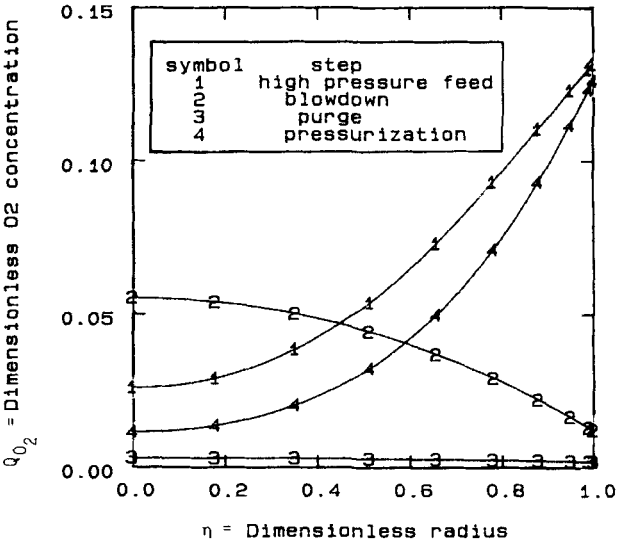

Figure 5. Dimensionless O_2 concentration within an adsorbent particle at cyclic steady state at end of respective steps.
Dimensionless bed length = 0.6193

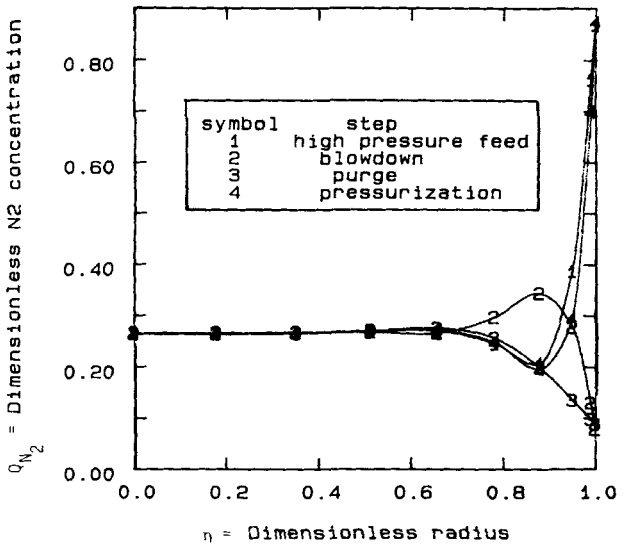

Figure 6. Dimensionless N_2 concentration within an adsorbent particle at cyclic steady state at end of respective steps.

Dimensionless bed length = 0.6193

tion step is pushed out of the column as product. The effect of inlet velocity is shown in Table 2. Since the breakthrough curve for zeolite 4A resembles a simple wave, contrary to equilibrium-based separations in which concentration shock fronts are formed, the gradual increase in inlet velocity (for fixed duration) results in greater oxygen contamination for the product but increasing quantities of product. The increase in duration of this step (for fixed velocity) shows the same trend as seen in Table 3.

Effect of Duration of Blowdown Step. Since the adsorbed impurity, oxygen, diffuses out of the adsorbent during the blowdown step, a longer blowdown time (τ_2) results in a cleaner bed. The effect of blowdown time, for the cases of short and long purge times, on product purity is given in Table 4. The blowdown time has a significant effect on product purity for the case of short purge time, but it has very little effect for a long purge time. Thus, sufficient blowdown time is essential for minimizing the amount of product necessary for purging, which in turn maximizes recovery. Also, the results indicate that the purge

Table 2. Effect of Inlet Velocity During High-Pressure Feed Step

Inlet Veloc. v_H cm/s	Mole Frac. of Product $\bar{y}_{N_2 p}$	Net Product Ratio
16	0.98483	1
21	0.97305	5.91
23	0.96822	7.88

Parameter values
$Pe = 400$ $\quad$ II = 11
$\tau_1 = 0.03$ $\quad$ $\tau_2 = 0.5$
$\tau_3 = 0.7$ $\quad$ $\tau_4 = 0.1$
$\gamma_v = -0.1429$ $\quad$ $N_{Pu}/N_H = 0.3031$
$\gamma_D = 0.016$

Net product ratio is scaled to reflect the smallest amount of net product (i.e., total product minus purge requirement) as unity.

Table 3. Effect of Duration of High-Pressure Feed Step

Duration Time τ_1	Mole Frac. of Product $\bar{y}_{N_2 p}$	Net Product Ratio
	$v_H = 16$ cm/s	
0.03	0.97981	1
0.045	0.97248	1.78
	$v_H = 10.67$ cm/s	
0.045	0.99016	1
0.1	0.97462	11.54

Parameter values
$Pe = 400$ $\quad$ II = 11
$\tau_2 = 0.5$ $\quad$ $\tau_3 = 0.7$
$\tau_4 = 0.1$ $\quad$ $N_{Pu}/N_H = 0.07578$
$\gamma_D = 0.016$

Net product ratio is scaled to reflect the smallest amount of net product (i.e., total product minus purge requirement) as unity.

time is more important than the blowdown time for obtaining pure product, as discussed in the next section.

Effect of Purge Step Parameters. The function of the purge step is to clean the bed by purging the column with part of the product stream produced during the high-pressure feed step. The cleaner the bed becomes, the higher the purity of the product. The bed can be more thoroughly cleaned by simply using more purge gas, as shown in Table 5. In this case the amount of purge gas is increased by increasing the purge gas velocity, rather than the duration. Both of these should have similar effects because equilibrium, rather than rate effects, are dominant in this step. Despite that, the slow diffusion rate of oxygen and nitrogen on zeolite 4A suggests that the duration of the purge step is important for removing the impurity, oxygen. The effect of purging time on separation when using a given amount of purge gas is given in Table 6. The results show that a long purge time and low purge velocity give a purer product than a short purge time and high purge velocity. This means that enough purge time should be allowed for oxygen to diffuse out of the adsorbent, i.e., to approach equilibrium more closely.

Effect of Duration of Pressurization Step. The results for various durations of the pressurization step, τ_4, at cyclic steady state are given in Table 7. The first three results, which were obtained by keeping constant all parameters except pressuriza-

Table 4. Effect of Duration of Blowdown Step on Product Purity

Blowdown Time τ_2	Purge Time τ_3	Purge Veloc. v_L cm/s	Mole Frac. of Product $\bar{y}_{N_2 p}$
0.2	0.1	16	0.96054
0.5	0.1	16	0.96872
0.8	0.1	16	0.97201
0.2	0.7	2.2864	0.98207
0.5	0.7	2.2864	0.98483
0.8	0.7	2.2864	0.98562

Parameter values
$\gamma_D = 0.016$ $\quad$ II = 11
$Pe = 400$ $\quad$ $\tau_1 = 0.03$
$\tau_4 = 0.1$ $\quad$ $v_H = 16$ cm/s
$N_{Pu}/N_H = 0.3031$

Table 5. Effect of Purge Velocity on Separation

Purge Veloc. v_L cm/s	Mole Frac. of Product $\bar{y}_{N_2p}$	Net Product Ratio
0.5716	0.97981	6.594
1.1432	0.98214	4.727
2.2864	0.98483	1

Parameter values
$\gamma_D = 0.016$ $\Pi = 11$
$Pe = 400$ $\tau_1 = 0.03$
$\tau_2 = 0.5$ $\tau_3 = 0.7$
$\tau_4 = 0.1$ $v_H = 16$ cm/s
Net product ratio is scaled to reflect the smallest amount of net product (i.e., total product minus purge requirement) as unity.

tion time, show that as the duration increases, the purity decreases but the amount of product increases. A longer duration permits greater uptake of nitrogen, while in comparison oxygen is taken up nearly instantaneously. So, the gas phase becomes proportionally richer in oxygen, and a poorer separation occurs.

The last three entries in Table 7 show the effect of reducing the inlet velocity during the high-pressure feed step while also increasing the duration of the pressurization step. As can be seen, it is possible to maintain high product quality and to obtain higher quantities of product for longer pressurization times by reducing the velocity during the high-pressure feed step. The net effect is to prevent breakthrough of impure product by manipulating these variables together. The subtle effect that leads to both greater quality and quantity is that more nitrogen is adsorbed during the longer pressurization step and it subsequently desorbs during blowdown. This partially cleanses the bed and supplements the purge step. Moreover, the combined effects of enhanced blowdown and prevention of breakthrough more than compensate for the potentially deleterious effect of a longer pressurization step mentioned in the previous paragraph.

Effect of Pressure Ratio. The effect of the pressure ratio, Π, on the separation is shown in Table 8. The purge velocity was changed to maintain a constant purge-to-feed ratio for all pressure ratios. The results show that even though the purity difference is not significant, the purity of product is maximized at $\Pi = 11$ for $P_L = 1$ bar. At $\Pi = 17$, however, during the initial several cycles a purer product was obtained than at cyclic steady state.

Table 6. Effect of Purge Time on Separation

Purge Time τ_3	Purge Veloc. v_L cm/s	Mole Frac. of Product $\bar{y}_{N_2p}$	Net Product Ratio
0.1	16	0.96872	2.677
0.4	4	0.98180	1.447
0.7	2.2864	0.98483	1

Parameter values
$\gamma_D = 0.016$ $\Pi = 11$
$Pe = 400$ $\tau_1 = 0.03$
$\tau_2 = 0.5$ $\tau_4 = 0.1$
$v_H = 16$ cm/s $N_{Pu}/N_H = 0.3031$
Net product ratio is scaled to reflect the smallest amount of net product (i.e., total product minus purge requirement) as unity.

Table 7. Effect of Duration of Pressurization Step

Pressurization Time τ_4	High-Pressure Feed Veloc. v_H cm/s	Mole Frac. of Product $\bar{y}_{N_2p}$	Net Product Ratio
0.1	16	0.98483	1
0.2	16	0.98250	4.837
0.3	16	0.98096	6.816
0.2	13	0.98869	1.901
0.3	12	0.98925	2.900
0.5	11	0.98935	4.040

Parameter values
$\gamma_D = 0.016$ $Pe = 400$
$\Pi = 11$ $\tau_1 = 0.03$
$\tau_2 = 0.5$ $\tau_3 = 0.7$
$\gamma_V = -0.1429$ $N_{Pu}/N_H = 0.3031$
Net product ratio is scaled to reflect the smallest amount of net product (i.e., total product minus purge requirement) as unity.

The cause of this subsequent decline was penetration of impure gas into the bed during the pressurization step. A higher pressure ratio results in a higher velocity due to a steeper pressure gradient with time. So, impure gas is pushed farther into the bed as the number of cycles increases, thus contaminating the product. For higher pressure ratios, the penetration may be limited by using a lower velocity or shorter duration for the high-pressure feed step. Those possibilities, however, were not analyzed fully in this work.

Effect of Pressurization Alternatives. Two pressurization methods are common in PSA separations: pressurization with feed, which is employed in the foregoing comparisons (step 4 in Figures 1A and 1B), and pressurization with product, which is the first alternative discussed here. For equilibrium-driven separations, an advantage of pressurization with product is that the recovery of the desired component is enhanced. This advantage, however, does not occur in air separation by zeolite 4A, as shown in Table 9. The purity of product for pressurization with product is uniformly lower than that for pressurization with feed. The reason for this poor separation is that the number of moles required for pressurization is large compared to the amount of product. This is due to the higher capacity of the adsorbent for nitrogen (than for oxygen) and the closer approach to equilibrium permitted by the time elapsed during pressurization. Therefore, pressurization with feed is more desirable than with product for nitrogen production by zeolite 4A.

Table 8. Effect of Pressure Ratio

Pressure Ratio Π	Purge Veloc. v_L cm/s	Mole Frac. of Product $\bar{y}_{N_2p}$
5	1.039	0.98218
11	2.286	0.98483
17	3.533	0.98086

Parameter values
$\gamma_D = 0.016$ $Pe = 400$
$\tau_1 = 0.03$ $\tau_2 = 0.5$
$\tau_3 = 0.7$ $\tau_4 = 0.1$
$v_H = 16$ cm/s $N_{Pu}/N_H = 0.3031$
$P_L = 1$ bar

Table 9. Effect of Pressurization with Product

τ_4	v_H cm/s	v_L cm/s	$\bar{y}_{N_2p}$	N_{Pr}/N_H	$(N_{Pr} + N_{Pu})/N_H$
0.05	64	2.286	0.99261	1.313	1.414
0.05	74	2.644	0.97958	1.102	1.199
0.01	77	0.393	0.96566	0.953	0.968
0.05	90	3.215	0.94581	0.898	0.971

Parameter values
$\gamma_D = 0.016$ $\Pi = 11$
$Pe = 400$ $\tau_1 = 0.03$
$\tau_2 = 0.5$ $\tau_3 = 0.7$

The second option considered here is vacuum swing adsorption, in which both P_L and P_H are lower absolute pressures than above but their ratio, Π, is unchanged. It was determined that there was no effect on the product purity for P_L in the range of 0.4 to 1.0 bar, because the isotherms were taken to be linear and because the effect of pressure on the mass transfer coefficients was ignored. Conversely, at low values of P_H attainment of cyclic steady state is more rapid, but the quantity of product is reduced.

Conclusions

A model has been developed in which all the major steps of a kinetically controlled PSA cycle can be taken into account. Results of the model include intraparticle and axial concentration profiles, as well as flow rates and product comparisons that are necessary to assess cycle performance. Major assumptions of the model include linear adsorption isotherms, isothermal operation, and restrictive mechanisms for diffusion.

A case study has been presented that explores several operating conditions for nitrogen separation from air with zeolite 4A. The purpose was to explain trends of results that were induced by systematically varying individual parameters, in order to gain an insight into operating policies. The results showed that a wide variety of conditions can be employed to obtain a product with a purity of at least 98 mol % nitrogen, in rough agreement with some commercial products.

Future work will be oriented toward selective extensions of the model to include a variety of steps and conditions for PSA cycles. In addition, experiments are planned to examine the system chosen for the current case study in order to test the predictions.

Acknowledgment

This research was partially sponsored by the United States Air Force Office of Scientific Research/AFSC, under contract. The support of K. G. Ikels of the School of Aerospace Medicine, Brooks AFB, Texas, is gratefully acknowledged.

Notation

C_i = concentration of component i in gas phase
$\bar{C}_i = C_i/C_H$
D_{ei} = effective intraparticle diffusivity of component i
D_L = axial dispersion coefficient
K_i = slope of equilibrium isotherm for component i
k_i = mass transfer coefficient of component i at particle surface
L = column length
N = moles of gas entering or leaving column during step indicated by subscript, e.g., Pu or Pr
P = total pressure in column
$\bar{P} = P/P_L$
Pe = Peclet number
$Q_i = q_i/K_iC_H$
q_i = intraparticle concentration of component i
R = gas constant
r = distance from center of spherical particle
r_o = particle radius
T = absolute temperature
t = time
t_j = duration of step j
v = interstitial velocity
$\bar{v} = v/v_H$
y_i = mole fraction of component i in gas phase
$\bar{y}_{N_2p}$ = average mole fraction of nitrogen in product
z = axial distance

Greek letters

ϵ_b = bed void fraction
$\eta = r/r_o$
$\chi = z/L$
$\tau = D_{eA}t/r_o^2$
$\tau_j = D_{eA}t_j/r_o^2$
$\tau_H = D_{eA}L/r_o^2v_H$
$\lambda_i = k_ir_o/D_{ei}K_i$
$\psi_i = K_i(1 - \epsilon_b)/\epsilon_b$
$\theta_A = v_Hr_o^2\epsilon_b/LD_{eA}K_A(1 - \epsilon_b)$
$\gamma_D = D_{eB}/D_{eA}$
$\gamma_v = v_L/v_H$
$\Pi = P_H/P_L$
Ω = proportionality parameter for linear driving force model

Subscripts

A = component A
B = component B
H = high-pressure feed step
i = component $i = A$ or B
j = step $j = 1$ to 4
L = low-pressure influent during purge
Pr = pressurization step
Pu = purge step
1 = high-pressure feed step
2 = blowdown step
3 = purge step
4 = pressurization step

Literature cited

Ball, D. J., "Comparison of the Static and Dynamic Sorption Capacities of 4A and 5A Zeolites," M.S. Thesis, Ohio State Univ. (1985).
Carter, J. W., and M. L. Wyszynski, "The Pressure Swing Adsorption Drying of Compressed Air," *Chem. Eng. Sci.*, **38**, 1093 (1983).
Chan, Y. N., F. B. Hill, and Y. W. Wong, "Equilibrium Theory of a Pressure Swing Adsorption Process," *Chem. Eng. Sci.*, **36**, 243 (1981).
Cheng, H. C., and F. B. Hill, "Recovery and Purification of Light Gases by Pressure Swing Adsorption," *Industrial Gas Separations*, T. E. Whyte, Jr., C. E. Yon, and E. H. Wagener, eds., *Amer. Chem. Soc. Symp. Ser.*, **223**, 195 (1983).
Chihara, K., and Suzuki, M., "Air Drying by Pressure Swing Adsorption," J. of Chem. Eng. of Japan, **16**, 293 (1983).
Do, D. D., and R. G. Rice, "Validity of the Parabolic Profile Assumption in Adsorption Studies," *AIChE J.*, **32**, 149 (1986).
Doong, S. J., and R. T. Yang, "Bulk Separation of Multicomponent Gas Mixtures by Pressure Swing Adsorption: Pore/Surface Diffusion and Equilibrium Models," *AIChE J.*, **32**, 397 (1986).
Flores Fernandez, G., and C. N. Kenney, "Modeling of the Pressure Swing Air Separation Process," *Chem. Eng. Sci.*, **38**, 827 (1983).
Ketter, R. L., and Prawel, S. P., "Modern Methods of Engineering Computation," McGraw Hill, New York (1969).
Knaebel, K. S., and F. B. Hill, "Pressure Swing Adsorption: Develop-

ment of an Equilibrium Theory for Gas Separations," *Chem. Eng. Sci.*, **40**, 2351 (1985).
Matz, M. J., and K. S. Knaebel, "Pressure Swing Adsorption: Temperature Front Sensing for Feed Step Control in a PSA Process," *Ind. Eng. Chem. Fundam.*, (submitted 1986).
Miller, G. W., K. S. Knaebel, and K. G. Ikels, "Adsorption Equilibria of Nitrogen, Oxygen, Argon and Air on Zeolite 5A," *AIChE J.*, **2**, 194 (1987).
Mitchell, J. E., and L. H. Shendalman, "A Study of Heatless Adsorption in the Model System CO_2 in He. II," *AIChE Symp. Ser.*, **69**, 25 (1973).
Nakao, S.-I., and M. Suzuki, "Mass Transfer Coefficient in Cyclic Adsorption and Desorption," *J. Chem. Eng. Japan*, **16**, 114 (1983).
Raghavan, N. S., and D. M. Ruthven, "Pressure Swing Adsorption. III: Numerical Simulation of a Kinetically Controlled Bulk Gas Separation," *AIChE J.*, **31**, 2017 (1985).
Raghavan, N. S., M. M. Hassan, and D. M. Ruthven, "Numerical Simulation of a PSA System. I: Isothermal Trace Component System with Linear Equilibrium and Finite Mass Transfer Resistance," *AIChE J.*, **31**, 385 (1985).
———, "Numerical Simulation of a PSA System using a Pore Diffusion Model," *Chem. Eng. Sci.*, **41**, 2787 (1987).
Ruthven, D. M., and R. I. Derrah, "Diffusion of Monatomic and Diatomic Gases in 4A and 5A Zeolites," *J. Chem. Soc. Faraday Trans. I*, **71**, 2031 (1975).
Shendalman, L. H., and J. E. Mitchell, "A Study of Heatless Adsorption in the Model System CO_2 in He. I," *Chem. Eng. Sci.*, **27**, 1449 (1972).
Shin, H.-S., Ph.D. Diss., "Pressure Swing Adsorption: A Study of Diffusion Induced Separations," Ohio State Univ. (in preparation, 1987).
Skarstrom, C. W., "Method and Apparatus for Fractionating Gas Mixtures by Adsorption," U.S. Patent 2,444,627 (1960).
Turnock, P. H., and R. H. Kadlec, "Separation of Nitrogen and Methane via Periodic Adsorption," *AIChE J.*, **17**, 335 (1971).
Villadsen, J. V., and M. L. Michelsen, *Solution of Differential Equation Models by Polynomial Approximation*, Prentice-Hall, Englewood Cliffs, NJ (1978).

Manuscript received June 11, 1986, and revision received Oct. 9, 1986.